AIP | The Journal of Chemical Physics

Molecular electronic states near metal surfaces at equilibrium using potential of mean force and numerical renormalization group methods: Hysteresis revisited

Wenjie Dou, Abraham Nitzan, and Joseph E. Subotnik

Citation: The Journal of Chemical Physics **144**, 074109 (2016); doi: 10.1063/1.4941848
View online: http://dx.doi.org/10.1063/1.4941848
View Table of Contents: http://scitation.aip.org/content/aip/journal/jcp/144/7?ver=pdfcov
Published by the AIP Publishing

Molecular electronic states near metal surfaces at equilibrium using potential of mean force and numerical renormalization group methods: Hysteresis revisited

Wenjie Dou,[1] Abraham Nitzan,[1,2] and Joseph E. Subotnik[1]
[1]*Department of Chemistry, University of Pennsylvania, Philadelphia, Pennsylvania 19104, USA*
[2]*School of Chemistry, The Sackler Faculty of Science, Tel Aviv University, Tel Aviv 69978, Israel*

(Received 13 November 2015; accepted 2 February 2016; published online 19 February 2016)

We investigate equilibrium observables for molecules near metals by employing a potential of mean force (PMF) that takes level broadening into account. Through comparison with exact data, we demonstrate that this PMF approach performs quite well, even for cases where molecule-electrode couplings depend on nuclear position. As an application, we reexamine the possibility of hysteresis effects within the Anderson-Holstein model (i.e., an impurity coupled both to a metal surface and a nuclear oscillator). As compared against the standard mean field approach by Galperin *et al.* [Nano Lett. **5**, 125 (2005)], our PMF approach agrees much better with exact results for average electronic populations both at zero and finite temperature; we find, however, that mean field theory can be very useful for predicting the onset of dynamical instabilities, metastable states, and hysteresis. © *2016 AIP Publishing LLC.* [http://dx.doi.org/10.1063/1.4941848]

I. INTRODUCTION

A lot of interesting physical phenomena have been observed in molecular junctions,[1–8] such as negative differential resistance (NDR),[9–11] bistability, and hysteresis.[12–14] To model NDR and hysteresis phenomena,[15] ten years ago, Galperin *et al.* applied a mean field approach to the Anderson-Holstein (AH) polaron model in the limit of strong metal-molecule coupling. (The AH model consists of an electronic impurity coupled both to a phonon and an electronic bath; see Eqs. (2)-(5) and Refs. 16–19.) The basic idea of a polaron model is that nuclear degrees of freedom can trap electrons in localized states. According to Galperin *et al.*, when treated with mean field theory (MFT), the AH model can yield multiple solutions for the electronic population that would indicate the existence of metastable electronic states (in analogy, for example, with the van der Waals equation of state of imperfect gases).

In agreement with MFT, real time numerical exact calculations such as Multi-Configuration Time-Dependent Hartree (MCTDH) and Diagrammatic Monte Carlo (DiagMC) also show signatures of bistability for the AH model,[20–22] with long- time populations dependent on the initial conditions. It should be emphasized that the existence of multiple solutions to such mean field equations does not imply the existence of multiple stable states (in a thermodynamic sense); rather the existence of such solutions implies only that the system can occupy such states for times that are long relative to typical observation times. Indeed, Rabani and co-workers[22,23] showed recently that the AH model admits only one truly equilibrium solution. In practice, the existence of multiple metastable states is often manifested in the existence of multiple peaks in the corresponding equilibrium distribution functions for some relevant observables.[24]

With this understanding in mind, the goal of the present article is to revisit the qualitative predictions of MFT and analyze those predictions in the context of two new and intuitive approaches that go beyond MFT for calculating equilibrium observables. By comparing results, we will be able to assess the accuracy of MFT and to learn how the signatures of multiple metastable states appear in the equilibrium solution. Let us now describe these two different approaches.

First, without a voltage bias, we will use numerical renormalization group (NRG) theory to study equilibrium populations in the AH model. When properly converged, NRG should yield exact solutions for any observable at equilibrium.[25–27] We will show below that when electron-phonon (e-ph) couplings are small, NRG and MFT agree well with each other. When e-ph couplings become large, MFT yields multiple solutions for the mean electronic population. As expected, NRG yields a single solution for the population, and that value exhibits a relatively sharp transition between the two stable branches obtained from the MFT calculation.

Second, further insight into the nature of this multistable region is obtained by studying the AH model with a potential of mean force (PMF) approach, in the spirit of the Born-Oppenheimer approximation. We define the potential of mean force using the electronic Hamiltonian (H_{el}, Eq. (11)) as

$$V(x) \equiv -\frac{1}{\beta} \ln\langle x|Tr_e e^{-\beta \hat{H}_{el}}|x\rangle. \tag{1}$$

Here, Tr_e implies tracing over all electronic degrees of freedom (DoFs), $|x\rangle$ represents an eigenstate of the position operator ($\hat{x}|x\rangle = x|x\rangle$), and β is the inverse temperature ($\beta \equiv 1/kT$). In the limit where electronic motion is much faster than nuclear motion, nuclei should evolve along such a potential of mean force, together with a random force and friction from

the electronic bath.[28–31] For large e-ph couplings, the PMF can exhibit multiple minima, which correspond to bistability and the possibility of transient switching between different states.[28,32] Below, we will quantify the noise in the electronic population that arises from these multiple minima. Thus, the multistable PMF allows us to hypothesize about hysteresis in the AH model and gives us a framework to interpret results from a MFT.

Now, while a PMF approach has been used before[28,32] to study the AH model with fully classical nuclei, in this paper, we will show that equilibrium electronic populations can be calculated using a PMF without needing to make a fully classical approximation for the nuclei. Furthermore, we will also show that our calculated PMF is in remarkable agreement with exact NRG calculations (as opposed to MFT). This agreement holds even when the molecule-electrode couplings depend on nuclear coordinates, which is very relevant for realistic systems. As such, we believe that this PMF approach should be very useful for modeling many coupled nuclear-electronic systems in the limit of fast electronic motion (large molecule-metal coupling); the method is not restricted to the AH model.

We organize the paper as follows. In Sec. II, we introduce the Anderson-Holstein model and motivate the problem. In Sec. III, we briefly review the standard MFT approach. In Sec. IV, we formulate the PMF approach. We show results in Sec. V, we revisit hysteresis in Sec. VI, and we conclude in Sec. VII. In Appendices A– F, we give further details of the PMF and NRG calculations, as well as an analysis of other, previously published approaches. In Appendices A– F, we also discuss the case of a position-dependent hybridization function.

II. ANDERSON-HOLSTEIN MODEL

We begin by briefly introducing the AH model. The AH model consists of an impurity level coupled both to one electrode (with a manifold of electronic states) and a single phonon. The Hamiltonian is

$$\hat{H} = \hat{H}_s + \hat{H}_b + \hat{H}_c. \tag{2}$$

Here, the system consists of the (electronic) impurity with creation (annihilation) operator $\hat{d}^+$ ($\hat{d}$) and energy level E_d, plus the phonon (nuclei) with position $\hat{x}$ and momentum $\hat{p}$,

$$\hat{H}_s = E_d \hat{d}^+\hat{d} + \sqrt{2} g \hat{x} \hat{d}^+\hat{d} + \frac{1}{2}\hbar\omega(\hat{x}^2 + \hat{p}^2). \tag{3}$$

Here, we choose $\hat{x}$ and $\hat{p}$ to be unitless. The bath (electrode) consists of a manifold of noninteracting electrons,

$$\hat{H}_b = \sum_k \epsilon_k \hat{c}_k^+ \hat{c}_k. \tag{4}$$

The system-bath coupling is bilinear with constant coefficients (V_k) by construction,

$$\hat{H}_c = \sum_k V_k(\hat{d}^+\hat{c}_k + \hat{c}_k^+\hat{d}). \tag{5}$$

The AH model can be considered the natural extension of the famous spin-boson model to the case of infinitely many (rather than two) electronic states; whereas the usual Marcus-Jortner theory of electron transfer can be derived from the spin-boson model,[33–36] Marcus' theory of electron transfer at a metal surface can be derived from the AH model.[37–39] Thus, for studying charge transfer near a metal surface, it is crucial that we have tools for solving the AH model. Just as for the spin-boson Hamiltonian, there is no general analytic solution for the AH model; we now discuss several approaches.

III. MFT

To model the dynamics of the AH model, MFT offers one approach. Let us briefly review the standard mean field approach following the work of Galperin *et al.*[15]

Focusing on the nuclear Hamiltonian (the last two terms in Eq. (3)), we see that the nuclei feel a force exerted by the electronic system,

$$\hat{F} = -\sqrt{2} g \hat{d}^+\hat{d}. \tag{6}$$

For large molecule-metal couplings, the rate at which the molecule exchanges electrons with the metal is fast relative to the characteristic nuclear timescale ($\Gamma \gg \hbar\omega$). In this limit, $\hat{d}^+\hat{d}$ in Eq. (6) can be replaced by the average population $N \equiv \langle \hat{d}^+\hat{d} \rangle$ at any nuclear position. Thus, in this mean field approximation, the electron exerts a mean force on the nucleus which depends on the average electronic population, $\bar{F} = -\sqrt{2} g N$, and the average equilibrium position of the oscillator is

$$\langle x \rangle = -\sqrt{2}\frac{gN}{\hbar\omega}. \tag{7}$$

Using this average instead of the position operator $\hat{x}$ of the nuclei in Eq. (3), we arrive at a mean field Hamiltonian for modeling the electronic dynamics

$$\hat{H}_{el}^{MF} = (E_d - 2E_r N)\hat{d}^+\hat{d} + \sum_k \epsilon_k \hat{c}_k^+\hat{c}_k + \sum_k V_k(\hat{d}^+\hat{c}_k + \hat{c}_k^+\hat{d}). \tag{8}$$

Here, we have defined the reorganization energy $E_r \equiv \frac{g^2}{\hbar\omega}$.

Eq. (8) is just a simple resonant level model. At equilibrium, the electronic population is given by[40]

$$N = \int \frac{dE}{2\pi} \frac{\Gamma}{(E - E_d + 2E_r N)^2 + (\Gamma/2)^2} f(E), \tag{9}$$

where Γ is the hybridization function,

$$\Gamma(\epsilon) = 2\pi \sum_k |V_k|^2 \delta(\epsilon_k - \epsilon). \tag{10}$$

We assume the wide band approximation here, so that Γ is chosen as a constant.

Note that Eq. (9) depends on the parameters ω and g only through $E_r = g^2/\hbar\omega$. Also, in Eq. (9), the electronic population (N) has to be solved self-consistently. As shown in Ref. 15 and below, Eq. (9) has multiple solutions when E_r is large enough.

IV. A PMF APPROACH

We now introduce a second approach for calculating equilibrium observables for the AH model based on a PMF. In this section, we consider only the case of constant electron-metal coupling. See Appendix A for the case where the electron-metal coupling depends on nuclear position.

In the spirit of the Born-Oppenheimer treatment, we separate the total Hamiltonian into an electronic Hamiltonian plus the nuclear kinetic energy,

$$\hat{H} = \hat{H}_{el} + \frac{1}{2}\hbar\omega\hat{p}^2. \tag{11}$$

The potential $\hat{H}_{el}$ and the associated force are relevant for the nuclear motion in the limit where the electronic exchange between the molecule and the metal (Γ of Eq. (10)) is much faster than the nuclear time scale determined by ω. As stated in Eq. (1), the PMF is defined as

$$V(x) \equiv -\frac{1}{\beta}\ln\langle x|Tr_e e^{-\beta\hat{H}_{el}}|x\rangle = -\frac{1}{\beta}\ln Tr_e e^{-\beta\hat{H}_{el}(x)}. \tag{12}$$

To calculate the PMF $V(x)$, we take the derivative of $V(x)$ over x, and get

$$\frac{\partial V(x)}{\partial x} = \frac{Tr_e(\hbar\omega x + \sqrt{2}g\hat{d}^+\hat{d})e^{-\beta\hat{H}_{el}(x)}}{Tr_e e^{-\beta\hat{H}_{el}(x)}} = \hbar\omega x + \sqrt{2}gn(x). \tag{13}$$

We have defined the population $n(x)$ as

$$n(x) \equiv \frac{Tr_e\hat{d}^+\hat{d}e^{-\beta\hat{H}_{el}(x)}}{Tr_e e^{-\beta\hat{H}_{el}(x)}}. \tag{14}$$

The local population $n(x)$ corresponds to a single level coupled to a continuum, and the single level has energy $\epsilon(x)$, where

$$\epsilon(x) = E_d + \sqrt{2}gx. \tag{15}$$

For such a problem, $n(x)$ can be expressed explicitly (just as in Eq. (9)) as[40]

$$n(x) = \int \frac{dE}{2\pi}\frac{\Gamma}{(E-\epsilon(x))^2 + (\Gamma/2)^2}f(E), \tag{16}$$

where f is the Fermi function of the electrode.

Note that using this equilibrium, electronic population at any nuclear position x is consistent with the timescale separation (fast electronic motion, slow nuclear motions, $\Gamma \gg \hbar\omega$) outlined above. Finally, we can integrate Eq. (13) to get the total PMF,

$$V(x) = \frac{1}{2}\hbar\omega x^2 + \sqrt{2}g\int_{-\infty}^{x} n(x')dx'. \tag{17}$$

The PMF in Eq. (17) will be the key quantity in all that follows below.

Next, the average electronic population N can be expressed as

$$N = \frac{1}{Z}\int dx\langle x|Tr_e\hat{d}^+\hat{d}e^{-\beta\hat{H}}|x\rangle = \frac{1}{Z}\int dx\frac{\langle x|Tr_e\hat{d}^+\hat{d}e^{-\beta\hat{H}}|x\rangle}{\langle x|Tr_e e^{-\beta\hat{H}}|x\rangle}\langle x|Tr_e e^{-\beta\hat{H}}|x\rangle. \tag{18}$$

Z is a normalization factor, $Z = \int dx\langle x|Tr_e e^{-\beta\hat{H}}|x\rangle$. In the spirit of the adiabatic approximation, we can approximate

$$\frac{\langle x|Tr_e\hat{d}^+\hat{d}e^{-\beta\hat{H}}|x\rangle}{\langle x|Tr_e e^{-\beta\hat{H}}|x\rangle} \approx \frac{\langle x|Tr_e\hat{d}^+\hat{d}e^{-\beta\hat{H}_{el}}|x\rangle}{\langle x|Tr_e e^{-\beta\hat{H}_{el}}|x\rangle} = n(x). \tag{19}$$

Now we seek an approximation for $\langle x|Tr_e e^{-\beta\hat{H}}|x\rangle$. We consider two limits.

A. High temperature, $kT \gg \hbar\omega$

At a high temperature, i.e., $kT \gg \hbar\omega$, we approximate $\langle x|Tr_e e^{-\beta\hat{H}}|x\rangle \approx \langle x|Tr_e e^{-\beta\hat{H}_{el}}|x\rangle = \exp(-V(x)/kT)$. Thus, the average electronic population is

$$N = \frac{1}{Z}\int dx\, n(x)e^{-\beta V(x)} \tag{20}$$

with the normalization factor $Z = \int dx e^{-\beta V(x)}$.

To get some intuition about Eq. (20), we further consider the case $\Gamma \ll kT$, where level broadening can be safely ignored. In such a case, from Eqs. (16) and (17), we have

$$n(x) = f(\epsilon(x)), \tag{21}$$

$$V(x) = \frac{1}{2}\hbar\omega x^2 - \frac{1}{\beta}\ln(1+\exp(-\beta\epsilon(x))), \tag{22}$$

and we can get a simple form for the electronic population

$$N = f(\bar{E}_d), \tag{23}$$

where $\bar{E}_d \equiv E_d - g^2/\hbar\omega$ is the renormalized impurity energy. Eq. (23) agrees with Eq. (E5) in Appendix E which was discussed in previous publications.[39,41,42] Moreover, in Ref. 42, we showed that, at a high temperature, the unbroadened PMF in Eq. (22) was consistent with a classical master equation.

B. Low temperature, $\hbar\omega \gg kT$

At low temperature, we make the following approximation,

$$\langle x|Tr_e e^{-\beta\hat{H}}|x\rangle \approx \langle x|\exp(-\beta\hat{h})|x\rangle = \sum_i \langle x|\psi_i\rangle\langle\psi_i|x\rangle\exp(-\beta E_i), \tag{24}$$

where $\hat{h}$ is the effective Hamiltonian for the oscillator and E_i and ψ_i are the eigenvalues and eigenstates of $\hat{h}$,

$$\hat{h} = V(x) + \frac{1}{2}\hbar\omega\hat{p}^2, \tag{25}$$

$$\hat{h}|\psi_i\rangle = E_i|\psi_i\rangle. \tag{26}$$

$V(x)$ is given by Eq. (17). We can then approximate the electronic population to be

$$N = \frac{1}{Z}\int dx\, n(x)\sum_i \psi_i^*(x)\psi_i(x)\exp(-\beta E_i), \tag{27}$$

with the normalization factor $Z = \sum_i \exp(-\beta E_i)$. At zero temperature, $N = \int dx\; n(x)\psi_0^*(x)\psi_0(x)$, where $\psi_0(x)$ is the ground state wave function.

In Appendix B, we show that, in both the cases (i.e., high temperature and low temperature), the relationship $N = \langle x\rangle/x_1$

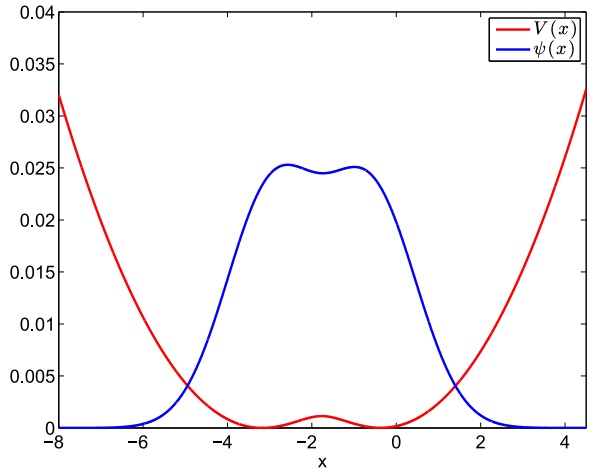

(a) $\bar{E}_d = 0$

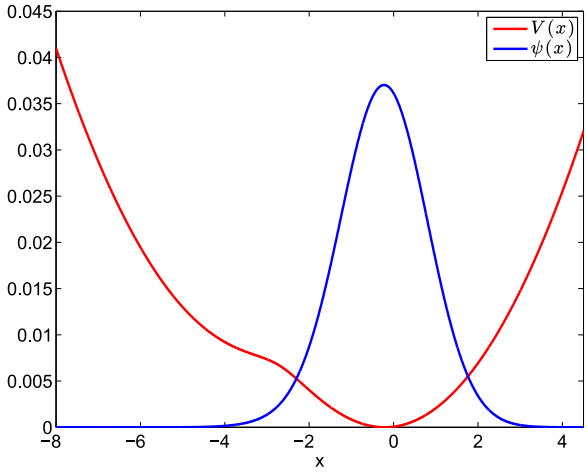

(b) $\bar{E}_d = 0.01$

FIG. 1. Potential of mean force $V(x)$ (from Eq. (17)) and ground state wave function (from Eq. (26)): $\Gamma = 0.01$, $\hbar\omega = 0.003$, $g = 0.0075$, $T = 0$.

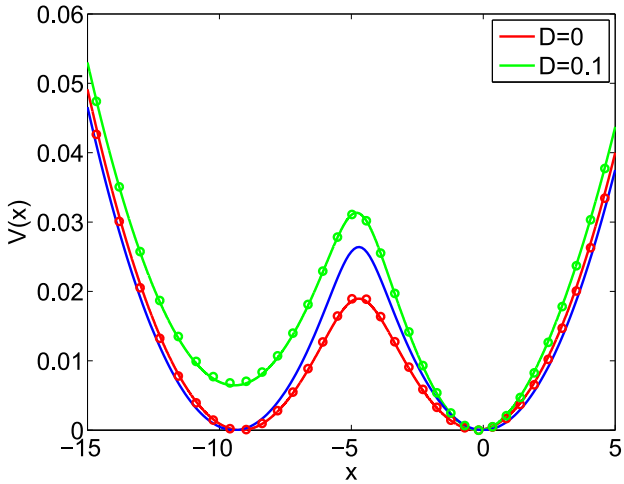

(a)

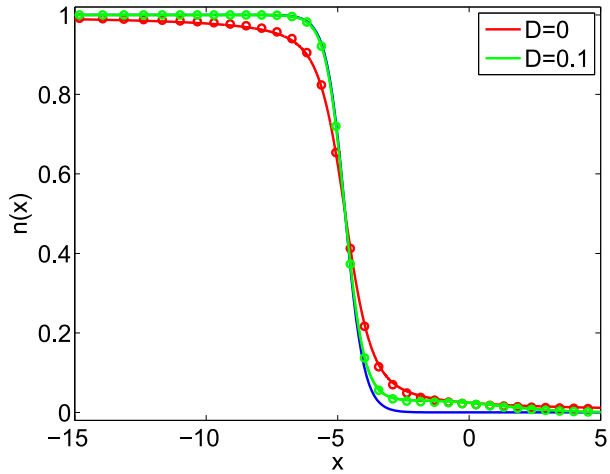

(b)

FIG. 2. (a) The potential of mean force $V(x)$ and (b) the local electronic population $n(x)$ as calculated by NRG[44] (circles) and our local approach (Eqs. (16) and (17)) (lines): $kT = 0.01$, $\Gamma_0 = 0.02$, $\hbar\omega = 0.003$, $g = 0.02$, $\bar{E}_d = 0$. Note the excellent agreement. Blue lines represent no broadening at all (Eq. (22) for $V(x)$ and Eq. (21) for $n(x)$). The parameter D represents a non-constant hybridization function. For the AH model with constant Γ, D = 0. See Appendix A (Eq. (A2)) for the full definition of D. The bandwidth is $2W = 2$.

holds, where $x_1 \equiv -\sqrt{2}g/\hbar\omega$ is the center of the shifted potential surface (the unshifted potential surface is centered at $x = 0$). This equality is one of the assumptions in the usual mean field approach (see Eq. (7)).

In Fig. 1, we plot the PMF and ground state wave function for the oscillator at $T = 0$ using Eqs. (25) and (26). The effective Schrödinger equation (Eq. (26)) is solved using an equally spaced grid.[43]

This concludes our discussion of the PMF approach. Below, we will analyze the value of this PMF approach and the resulting wave functions for understanding many different parameter regimes for the AH model; we will compare against exact NRG calculations.

V. RESULTS

A. Local population n(x) and the potential of mean force V(x)

Before addressing the average electronic population, in Fig. 2, we compare the local electronic population $n(x)$ and the PMF $V(x)$ according to both NRG and our local approach (Eqs. (16) and (17)).

Recall that NRG is an exact approach for diagonalizing the many body Hamiltonian of the AH form.[25–27] Now, in Section IV, we defined the local electronic population and PMF using the *electronic* Hamiltonian which depended on nuclear position (see Eqs. (12) and (14)). By contrast, for NRG, one can define the exact PMF and local electronic population by using the *total* Hamiltonian in the definition of $V_{NRG}(x)$ and $n_{NRG}(x)$,

$$V_{NRG}(x) = -\frac{1}{\beta}\ln\langle x|Tr_e e^{-\beta\hat{H}}|x\rangle, \tag{28}$$

$$n_{NRG}(x) = \frac{\langle x|Tr_e \hat{d}^+\hat{d}e^{-\beta\hat{H}}|x\rangle}{\langle x|Tr_e e^{-\beta\hat{H}}|x\rangle}. \tag{29}$$

The exact average electronic population is given by $N = \frac{1}{Z}\int dx\ n_{NRG}(x)\exp(-\beta V_{NRG}(x))$. Details can be found in Appendix D. From Fig. 2, it is clear that the $V(x)$ and $n(x)$ as calculated by NRG agree with our PMF approach nearly perfectly.

B. Average electronic population

We now compare results for average electronic population as calculated with different approaches: MFT, NRG, and our PMF approach (at low or high temperature). For comparison, we also plot results without any broadening at all (which is a simple Fermi function [Eq. (23)]), and two previously published *ad hoc* recipes for including broadening on top of a surface hopping (SH)/classical master equation (CME) calculation: broadening by Γ ("broadening 1") and broadening by the Marcus rate ("broadening 2"). See Appendix E.

In Fig. 3, we consider the low temperature regime. We plot the average electronic population as a function of the renormalized impurity energy level at $T = 0$, according to NRG, mean field (MF) theory, our low-temperature PMF approach (Eq. (27)), and broadening by Γ ("broadening 1"). We note that the PMF approach agrees with NRG very well for either small or large e-ph couplings. By contrast, for large e-ph couplings, MF gives multiple solutions. As discussed above, these multiple solutions represent the locally stable states associated with the minima in the potential of mean force and the barrier between them.

In Fig. 4, we consider the high temperature regime where $kT \gg \hbar\omega$. Again, we plot the average electronic population as a function of the renormalized impurity energy level. When the e-ph coupling g is small, all broadening approaches work equally well. When g gets larger, however, our PMF approach (Eq. (20)) works the best among all the different broadening procedures, agreeing with NRG nearly exactly. As before, MF finds multiple solutions (locally stable states)

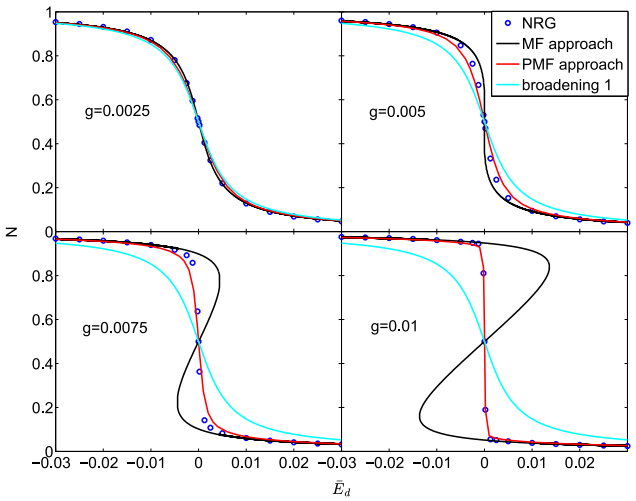

FIG. 3. Electron population as a function of $\bar{E}_d = E_d - g^2/\hbar\omega$. $\Gamma = 0.01$, $\hbar\omega = 0.003$, $kT = 0$. Broadening 1 refers to *ad hoc* broadening by Γ; see Eq. (E6). Notice that mean field (MF) theory (Eq. (9)) predicts spurious multiple solutions, whereas the PMF approach (Eqs. (16), (17), and (27)) is quite accurate. The NRG data can be considered exact.[44]

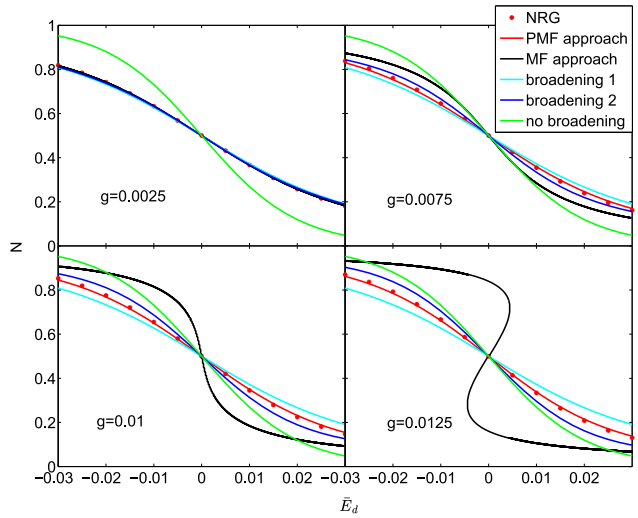

FIG. 4. Electron population as a function of renormalized impurity level $\bar{E}_d = E_d - g^2/\hbar\omega$. $\Gamma = 0.03$, $\hbar\omega = 0.003$, $kT = 0.01$. Broadening 1 refers to *ad hoc* broadening by Γ; see Eq. (E6). Broadening 2 refers to *ad hoc* broadening by the Marcus rate; see Eq. (E7). The NRG data can be considered exact.[44] Notice that the PMF approach (Eqs. (16), (17), and (20)) continues to be quite accurate, unlike MF theory (Eq. (9)).

for large e-ph couplings. Note also that increasing g tends to reduce the broadening effect (as discussed in Ref. 39). While broadening by the Marcus rate ("broadening 2") is sensitive to the dependence of broadening on electron-phonon coupling, we find that often such an approach implies too little broadening.

VI. DISCUSSION

A. Hysteresis revisited: Population noise from the PMF calculation

The results in Figs. 3 and 4 have shown that the MF electronic populations do not represent the long-time average of this population but rather provide approximations to the average populations associated with relatively long-lived locally stable states. The signature of such states is often seen in experiments when a control parameter (such as gate potential) changes on a time scale shorter than these lifetimes, and transitions between states then assume hysteretic character. In the opposite case—where the system is sampled for a long time (longer than the switching time between the locally stable states)—only a single value is found for average population.

Let us now be more quantitative. For the set of parameters in Fig. 2(a), we find a PMF with double well character and a large barrier (larger than kT) between the left and right wells, which indicates that for large values of Γ, where the system dynamics move along the PMF,[28,42] the distribution of molecular states will be double peaked and the neighborhoods of these peaks correspond to relatively long-lived metastable states. To quantify the noise in the population, we define the probability density of the population $\rho_h(\tilde{N})$,

$$\rho_h(\tilde{N}) = \int dx \rho(x)\delta(n(x) - \tilde{N}). \tag{30}$$

As discussed above, in the high temperature limit (and as a function of position), $\rho(x) = \frac{1}{Z}e^{-\beta V(x)}$; in the low temperature limit, $\rho(x) = \frac{1}{Z}\sum_i \psi_i^*(x)\psi_i(x)\exp(-\beta E_i)$. In Fig. 5(a), we plot $\rho_h(\tilde{N})$ for a symmetric system ($\bar{E}_d = 0$). Note that, as the e-ph coupling (g) increases, $\rho_h(\tilde{N})$ becomes more and more bimodal (and so does the PMF).

Finally, we may now further define the population noise to be the variance of the population probability density,

$$\langle \Delta N^2 \rangle = \langle \tilde{N}^2 \rangle - \langle \tilde{N} \rangle^2 = \int d\tilde{N}\rho_h(\tilde{N})\tilde{N}^2 - \left(\int d\tilde{N}\rho_h(\tilde{N})\tilde{N} \right)^2$$

$$= \int dx\, n^2(x)\rho(x) - \left(\int dx\, n(x)\rho(x) \right)^2. \quad (31)$$

As we can see from Fig. 5(b), increasing g leads to an increases in the population noise.

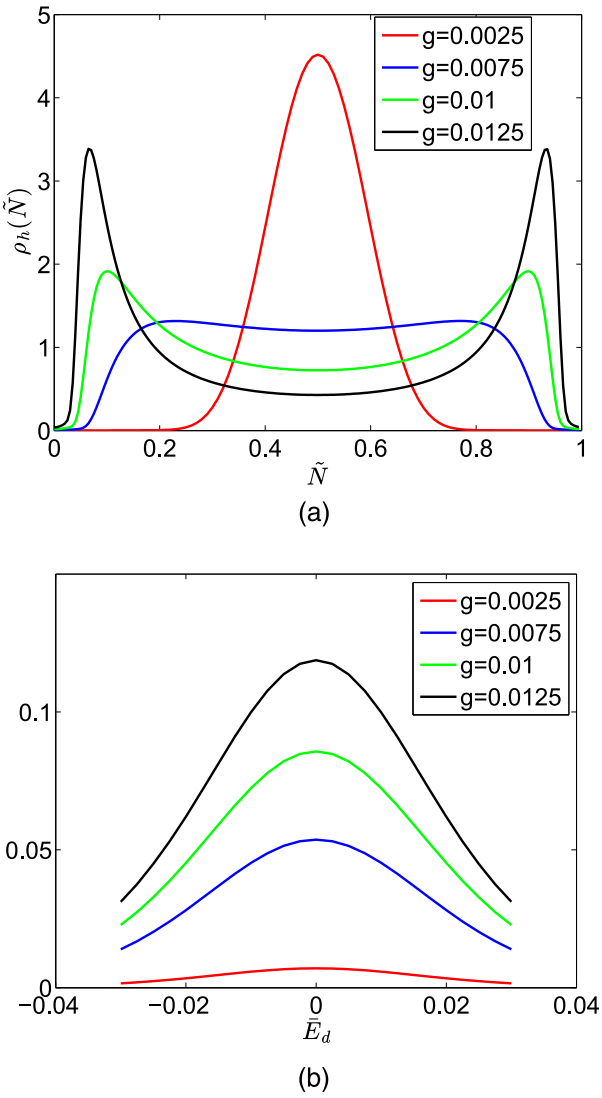

FIG. 5. (a) The probability density $\rho_h(\tilde{N})$ for the electronic population for a symmetric well ($\bar{E}_d = 0$); see Eq. (30). (b) Population noise $\langle \Delta N^2 \rangle$ as a function of $\bar{E}_d = E_d - g^2/\hbar\omega$ (Eq. (31)). For both calculations, $\Gamma = 0.03$, $\hbar\omega = 0.003$, $kT = 0.01$. Notice that increasing the e-ph coupling g forces the probability density to become more and more bimodal and thus increases the population noise.

B. Hysteresis revisited: The value of a MFT calculation

Let us now examine how much of the underlying physics of metastable states and hysteresis can be extracted for a MF calculation. In Fig. 6, we plot the height of the PMF energy barrier as a function of e-ph coupling g for the symmetric case $E_d = E_r$. According to our calculations, the energy barrier becomes positive around $g = 0.01$. In fact, in Appendix F, we prove that for the symmetric case in Fig. 6, the critical value of g (above which one finds multiple solutions for the electronic population in a MFT) is exactly the same value of g that gives a finite (nonzero) energy barrier according to a potential of mean force.

Let us now be a bit more quantitative and consider the asymmetric case. To further understand the hysteresis in the MF results, we define relative left and right electronic populations (N_l and N_r)

$$N_l = \frac{\int_{-\infty}^{x_{1/2}} n(x)e^{-\beta V(x)}dx}{\int_{-\infty}^{x_{1/2}} e^{-\beta V(x)}dx}, \quad (32)$$

$$N_r = \frac{\int_{x_{1/2}}^{\infty} n(x)e^{-\beta V(x)}dx}{\int_{x_{1/2}}^{\infty} e^{-\beta V(x)}dx}. \quad (33)$$

In Fig. 7(a), we plot N_l and N_r as a function of the impurity level $\bar{E}_d$. Note that for some values of $\bar{E}_d$, the PMF shows a double well (as in Fig. 7(b) middle panel); for other values, the PMF shows a single well either on the left (as in Fig. 7(b) left panel) or on the right (as in Fig. 7(b) right panel). We use different colors to distinguish these cases. Clearly, as calculated by a PMF, N_l and N_r are in near agreement with MF results provided that the total PMF is not a single well situated at the opposite position in space.

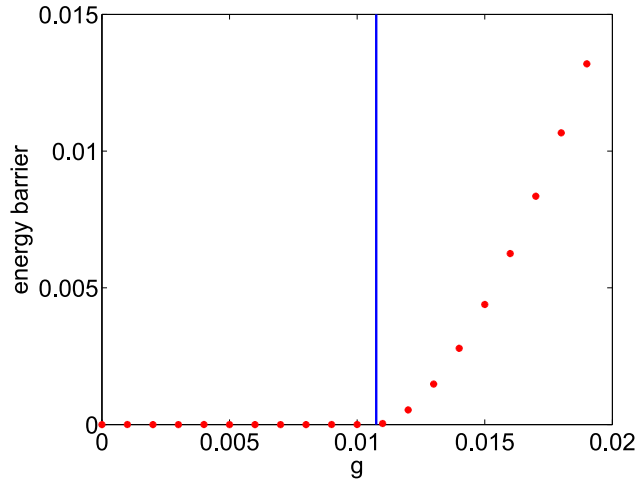

FIG. 6. (Red dots) The energy barrier of the potential of mean force near the crossing point between left and right wells (as calculated with our PMF approach [Eqs. (16) and (17)]). The blue line denotes the critical value of g above which we find multiple solutions for electronic population at the MF level (Eq. (9)). $\bar{E}_d = 0$, $\Gamma = 0.03$, $\hbar\omega = 0.003$, $kT = 0.01$. As proven in Appendix F, for symmetric systems like these (with $\bar{E}_d = 0$), the onset of an energetic barrier for the PMF is exactly the onset of multiple solutions in Galperin's MFT, suggesting that MFT could well be useful for predicting dynamical instability.

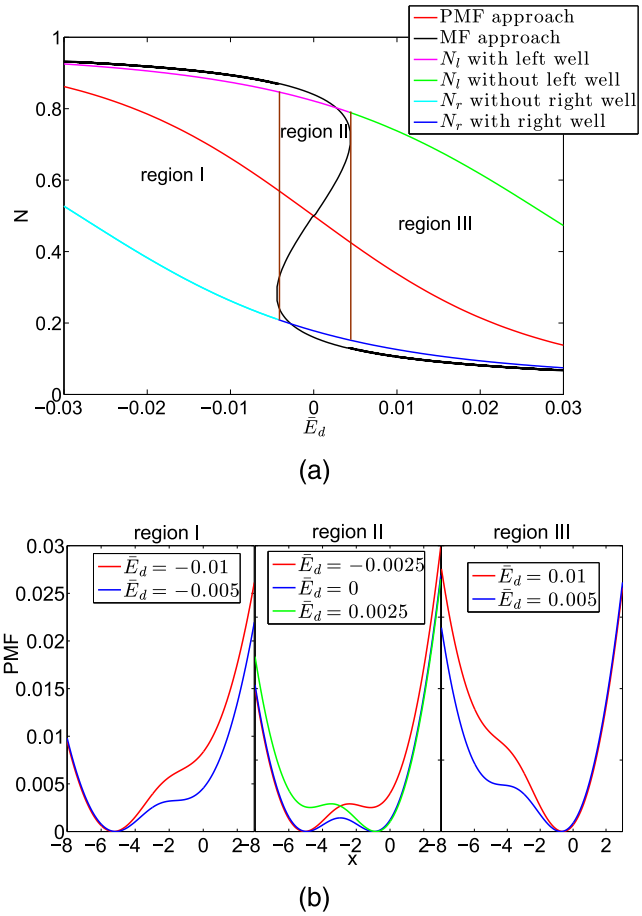

FIG. 7. (a) Relative left and right electronic population N_l, N_R (see Eqs. (32) and (33)) as a function of renormalized energy level $\bar{E}_d$. We also plot the electronic population according to our PMF approach (Eqs. (16), (17), and (20)) and MF theory (Eq. (9)). (b) The potential of mean force for the different regions labeled in subplot (a). In region I ($\bar{E}_d < -0.004$ roughly), there is only a left well. In region II ($-0.004 < \bar{E}_d < 0.004$ roughly), the PMF has a double well. In region III ($\bar{E}_d > 0.004$ roughly), there is only a right well. N_l and N_r are in near agreement with MF results provided that the total PMF is not a single well situated at the opposite position in space. $g = 0.0125$, $\Gamma = 0.03$, $\hbar\omega = 0.003$, $kT = 0.01$.

In the end, we may conclude that, while the average populations obtained from MF theory do not correspond to absolute long time averages, their behavior yields a diagnostic tool for understanding hysteresis and, if properly interpreted, can even be semi-quantitative.

C. Outlook for dynamical implications

The data above have shown that a PMF approach can be quite accurate for calculating equilibrium observables, and MFT can be useful as well if properly interpreted. Before concluding, we now want to say a few words about moving beyond equilibrium observables and calculating dynamics. Obviously, modeling molecular dynamics near metals is very difficult. One must take into account nuclear motion, electronic motion, and the coupling therein, and there is no simple set of equations for describing coupled nuclear electronic dynamics for all parameter regimes. A nearly exact treatment of this problem[45] yields a rather involved set of integro-differential equations.

In the present paper, we have mostly followed the work of Ref. 28, where the authors always assume that nuclear motion (as characterized by a nuclear frequency ω) is much slower than electronic motion (as characterized by the inverse lifetime Γ), $\omega \ll \Gamma$. In this limit, one can model dynamics on a single PMF with frictional damping and a random force.[28,42] Within the context of this assumption, one can make a few rough predictions about dynamics. For example, using the PMF in Fig. 7 for the AH model, one can estimate the time scale for switching of the electronic states as follows. For the case of moderate friction (either from the electronic bath or an external phonon bath), and only one electronic bath at equilibrium, the switching rate can be estimated as a barrier crossing problem using transition state theory in the high temperature limit,

$$1/\tau_{thermal} \approx \frac{\omega}{2\pi} \exp\left(-\frac{U_{barrier}}{kT}\right), \tag{34}$$

where $U_{barrier}$ is the barrier height of the PMF. In low temperature limit (as for the case in Refs. 22 and 23), Ref. 46 argues that the switching rate should take the form

$$1/\tau_{quantum} \approx \frac{\omega}{2\pi} \exp\left(-\frac{U_{barrier}}{\hbar\omega/2\pi}\right), \tag{35}$$

to account for quantum tunneling.

Now, if we look forward to more general and realistic systems, the assumption $\Gamma \gg \hbar\omega$ might be considered a limitation of the usual PMF approach. That being said, over the last year or so, we have been studying a different limit, where the assumption is that inverse electronic lifetime Γ is smaller than the temperature of the metal electrode kT.[39,41,42] In such a case, using Redfield theory, one can derive Eqs. (E1) and (E2) of Appendix E which are a CME, according to which a classical particle moves on two diabatic potential energy surfaces (PES's) with stochastic hops between the two PES's. In this limit, provided $\omega \ll \Gamma$, we do recover the picture of nuclei moving along potentials of mean force with electronic friction and random forces.[42] However, in Ref. 42, we worked with an unbroadened PMF, as opposed to the PMF's studied by von Oppen *et al.* in Ref. 28 which are broadened (as in Eq. (17)). Thus, the present paper (see Eq. (17)) provides a framework for including broadening on top of the CME and modeling molecular dynamics for many molecules near or far from metal surfaces. Such a dynamical algorithm was recently published.[47]

VII. CONCLUSIONS

We have presented a PMF approach for calculating equilibrium observables as relevant to electronic impurities near metal surfaces, and compared its performance with NRG calculations. This PMF approach is quite general, and should be easily applicable to multi-dimensional problems with many nuclear degrees of freedom, where the potential energy surfaces are not quadratic and the hybridization function is not a constant.

In the present paper, we have studied variations of the AH model, where exact results can be calculated with NRG. The results from the PMF approach agree well with NRG results for both zero T and finite T. Furthermore, when generalized to treat the case whereby Γ depends on nuclear position, our PMF approach gives excellent agreement with NRG (see Appendix A). Overall, when e-ph coupling gets large, the PMF approach outperforms MFT as well as any *ad hoc* broadening formalism. As such, we believe that the PMF approach described here should be an effective way to calculate equilibrium quantities. Its application to dynamics is, however, restricted to the $\Gamma \gg \hbar\omega$ regime.

Regarding hysteresis, we have shown that for symmetric cases, the potential of mean force energy develops a barrier exactly when MF theory predicts multiple solutions for the electronic population. Furthermore, we showed that, when interpreted correctly, MF theory can be useful in explaining the onset of hysteresis—though MF theory will not be quantitatively accurate or complete.

Looking forward, given that we can use our PMF approach to tackle problems where Γ depends on position x (as shown in Appendix A), in the future, it will be very interesting to investigate the effect of non-Condon terms on the friction and random force felt by a molecule near an electronic bath.[28,42] Furthermore, because our PMF approach is not restricted by any harmonic approximations, this algorithm should be very useful for calculating the equilibrium electronic properties for realistic systems. The most pressing question now is how to parameterize system-bath models with free metallic electrons using *ab initio* electronic structure theory: this work is ongoing.

ACKNOWLEDGMENTS

This material is based upon work supported by the (U.S.) Air Force Office of Scientific Research (USAFOSR) PECASE award under AFOSR Grant No. FA9950-13-1-0157. J.E.S. acknowledges a Cottrell Research Scholar Fellowship and a David and Lucille Packard Fellowship.

APPENDIX A: Γ DEPENDS ON NUCLEAR POSITION x

For the most of this paper, we have assumed that the hybridization function Γ was a constant. Let us now extend the AH model to the case where the metal-molecule coupling, Γ depends on the nuclear position, i.e., $\Gamma(x)$. Without loss of generality, in the following, we investigate the specific case whereby

$$\hat{H}_c = \sum_k V_k \exp(-D\hat{x}^2/2)(\hat{d}^+\hat{c}_k + \hat{c}_k^+\hat{d}). \tag{A1}$$

All V_k terms are independent of x, so that

$$\Gamma = 2\pi \sum_k V_k^2 \delta(\epsilon - \epsilon_k) \exp(-D\hat{x}^2) = \Gamma_0 \exp(-D\hat{x}^2), \tag{A2}$$

where Γ_0 is assumed to be a constant.

To define the PMF $V(x)$ (Eq. (12)), as before, we take the derivative of $V(x)$ as a function of x,

$$\frac{\partial V(x)}{\partial x} = \frac{Tr_e(\hbar\omega x + \sqrt{2}g\hat{d}^+\hat{d} - Dx\sum_k V_k \exp(-Dx^2/2)(\hat{d}^+\hat{c}_k + \hat{c}_k^+\hat{d}))e^{-\beta\hat{H}_{el}(x)}}{Tr_e e^{-\beta\hat{H}_{el}(x)}} = \hbar\omega x + \sqrt{2}gn(x) - DxY(x). \tag{A3}$$

Here, we see the appearance of a new, additional term $-DxY(x)$, where

$$Y(x) = \frac{Tr_e \sum_k V_k \exp(-Dx^2/2)(\hat{d}^+\hat{c}_k + \hat{c}_k^+\hat{d})e^{-\beta\hat{H}_{el}(x)}}{Tr_e e^{-\beta\hat{H}_{el}(x)}}. \tag{A4}$$

Using a Green's function formalism for a fixed x, this term can be explicitly written as (see Appendix C)[40]

$$Y(x) = 2\int \frac{dE}{2\pi} \frac{(E - \epsilon(x))}{(E - \epsilon(x))^2 + (\Gamma/2)^2} \Gamma f(E), \tag{A5}$$

where $\epsilon(x)$ is defined in Eq. (15).

Note that the integral in Eq. (A5) diverges logarithmically if we integrate over E from $-\infty$ to ∞. Thus, clearly, we cannot make the wide band approximation when evaluating this term; the bandwidth $2W$ (from $-W$ to W) must enter here explicitly:

$$Y(x) = 2\int_{-W}^{W} \frac{dE}{2\pi} \frac{(E - \epsilon(x))}{(E - \epsilon(x))^2 + (\Gamma/2)^2} \Gamma f(E). \tag{A6}$$

As such, for a position dependent hybridization function, the potential of mean force will necessarily depend on the bandwidth: the wide band approximation is impossible. Indeed, in Fig. 8, we show that the exact solution (obtained by numerical renormalization group) does depend on bandwidth, in agreement with Eq. (A6).

In Fig. 8, we plot the potential of mean force for several different values of the bandwidth W for the case that Γ depends on position x. As discussed above, because of the extra $Y(x)$ term in Eq. (A6), the PMF will necessarily be sensitive to the bandwidth of the metal (i.e., one cannot make a wide band approximation). If Γ is a constant, there is no such $Y(x)$ term and hence the PMF will not depend on bandwidth W (as long as W is large enough such that the wide band approximation applies). Note that our PMF approach agrees nearly exactly with NRG for all values of the bandwidth.

In Fig. 9, we plot the average electronic population for the case where $\Gamma = \Gamma_0 \exp(-Dx^2)$, so that one violates the Condon approximation. As the figure shows, the electronic

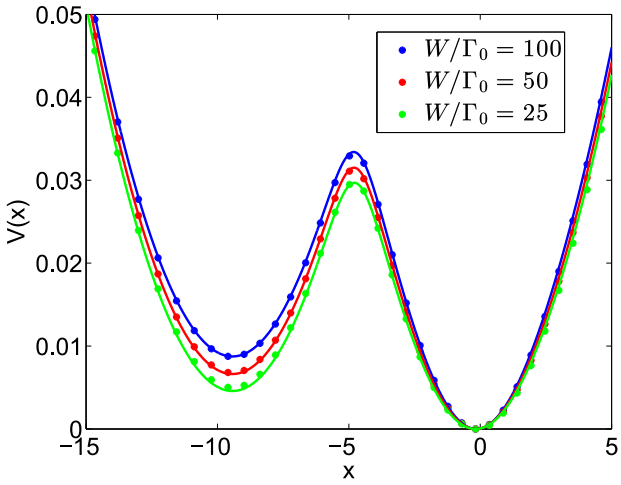

FIG. 8. The potential of mean force $V(x)$ from NRG[44] (dots) and our local approach Eq. (A3) (lines): $\Gamma = \Gamma_0 \exp(-Dx^2)$, $\Gamma_0 = 0.02$, $D = 0.1$, $kT = 0.01$, $\hbar\omega = 0.003$, $g = 0.02$, $\bar{E}_d = 0$. Note the agreement between NRG and Eq. (A3). Also, note that the potential of mean force depends on the bandwidth $2W$ when D is nonzero. No such dependence has been found when $D = 0$ (not shown).

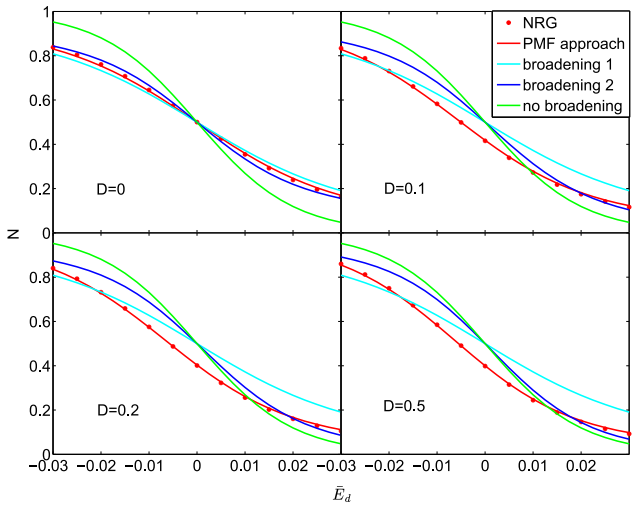

FIG. 9. Electron population as a function of the renormalized impurity level $\bar{E}_d = E_d - g^2/\hbar\omega$ for the case that the hybridization depends on position: $\Gamma_0 = 0.03$, $\Gamma = \Gamma_0 \exp(-Dx^2)$, $\hbar\omega = 0.003$, $kT = 0.01$, $g = 0.0075$. Here, Broadening 1 refers to *ad hoc* broadening by Γ_0; see Eq. (E6). Broadening 2 refers to *ad hoc* broadening by the Marcus rate; see Eq. (E7). NRG data can be considered exact.[44] Note that PMF data (Eqs. (20) and (A3)) are very accurate. If one ignores the $Y(x)$ term in Eq. (A3), however, the PMF data would become qualitatively incorrect (not shown). The bandwidth is $2W = 2$.

population as calculated by the PMF approach agrees with that from NRG almost exactly. Note, however, that, as discussed above, the PMF is irrelevant for the nuclear dynamics when Γ is not large in comparison with ω.

Finally, one word is in order about the relationship between nuclear position and electronic population. By comparison with Sec. IV, the reader should recognize that, because of the extra term $Y(x)$ in Eq. (A3), the relationship $N = \langle x \rangle / x_1$ does not hold when Γ depends on x (see Appendix B).

APPENDIX B: ESTABLISHING THE RELATIONSHIP BETWEEN THE AVERAGE ELECTRONIC POPULATION AND THE AVERAGE POSITION OF THE OSCILLATOR

Here, we prove that Eq. (7)—which was hypothesized for the MFT approach—also holds for our PMF approach.

At high temperature, we can write the expression for the electronic population (N) explicitly and integrate it by parts (where Z is the partition function),

$$N = \frac{1}{Z}\int dx\, n(x) \exp\left(-\frac{1}{2}\beta\hbar\omega x^2 - \sqrt{2}g\beta\int_{-\infty}^{x} n(x')dx'\right) = -\frac{1}{\sqrt{2}g\beta Z}\int \exp\left(-\frac{1}{2}\beta\hbar\omega x^2\right) d\exp\left(-\sqrt{2}g\beta\int_{-\infty}^{x} n(x')dx'\right)$$
$$= -\frac{\hbar\omega}{\sqrt{2}g}\frac{1}{Z}\int dx\, x \exp\left(-\frac{1}{2}\beta\hbar\omega x^2 - \sqrt{2}g\beta\int_{-\infty}^{x} n(x')dx'\right) = -\frac{\hbar\omega}{\sqrt{2}g}\langle x\rangle. \quad \text{(B1)}$$

This proves the relationship at high temperature.

At low temperature, we take the derivative of the effective Schrödinger equation (Eq. (26)) over x for both sides, and rearrange such that

$$\frac{\partial \hat{h}}{\partial x}\psi_i = (E_i - \hat{h})\frac{\partial}{\partial x}\psi_i. \quad \text{(B2)}$$

If we multiply Eq. (B2) by $\psi_i^*(x)$ and integrate it over x, we have

$$\int dx \psi_i^* \frac{\partial \hat{h}}{\partial x}\psi_i = \int dx \psi_i^* (E_i - \hat{h})\frac{\partial}{\partial x}\psi_i = 0. \quad \text{(B3)}$$

Here, we have used the fact that the Hamiltonian is Hermitian. With $\frac{\partial \hat{h}}{\partial x} = \hbar\omega x + \sqrt{2}gn(x)$ (Eq. (25)), again we arrive at

$$N = \frac{1}{Z}\int dx \sum_i \psi_i^*(x) n(x) \psi_i(x) \exp(-\beta E_i) \quad \text{(B4)}$$
$$= -\frac{\hbar\omega}{\sqrt{2}gZ}\int dx \sum_i \psi_i^*(x) x \psi_i(x) \exp(-\beta E_i) = \frac{\langle x\rangle}{x_1}. \quad \text{(B5)}$$

APPENDIX C: EVALUATING EQ. (A5)

For a single resonant level model, we have the following relationship:[48]

$$G^<_{d,c_k}(E) = \bar{V}_k (G^r_{d,d}(E) g^<_k(E) + G^<_{d,d}(E) g^a_k(E)), \quad \text{(C1)}$$

where $\bar{V}_k = V_k \exp(-Dx^2/2)$ and $G^<_{d,c_k}(E)$ is the Fourier transform of $G^<_{d,c_k}(t - t')$,

$$G^{<}_{d,c_k}(t-t') = i\langle \hat{c}^{+}_k(t')\hat{d}(t)\rangle. \tag{C2}$$

For a resonant level model, all the Green functions are known

$$G^{r}_{d,d}(E) = \frac{1}{E-\epsilon(x)+i\Gamma/2}, \tag{C3}$$

$$G^{<}_{d,d}(E) = i\frac{\Gamma}{(E-\epsilon(x))^2+(\Gamma/2)^2}f(E), \tag{C4}$$

$$g^{<}_{k}(E) = i2\pi\delta(E-\epsilon_k)f(\epsilon_k), \tag{C5}$$

$$g^{a}_{k}(E) = \frac{1}{E-\epsilon_k-i\eta}. \tag{C6}$$

So, $Y(x)$ can be expressed explicitly,

$$\begin{aligned} Y(x) &= \sum_k \bar{V}_k\langle \hat{d}^{+}\hat{c}_k + \hat{c}^{+}_k\hat{d}\rangle = 2\sum_k \bar{V}_k \int \frac{dE}{2\pi}\Re(-iG^{<}_{d,c_k}(E)) \\ &= 2\int \frac{dE}{2\pi}\frac{E-\epsilon(x)}{(E-\epsilon(x))^2+(\Gamma/2)^2}\Gamma f(E), \end{aligned} \tag{C7}$$

where we have used

$$2\pi\sum_k \bar{V}^2_k\delta(E-\epsilon_k)f(\epsilon_k) = \Gamma f(E), \tag{C8}$$

$$\Re\sum_k V^2_k\frac{1}{E-\epsilon_k-i\eta} = 0. \tag{C9}$$

The last equation corresponds to the wide band approximation.

APPENDIX D: DETAILS OF THE NRG CALCULATION

Recall that for a NRG calculation, in second quantization, the Hamiltonian is transformed into a semi-infinite chain of sites,

$$\hat{H} = \lim_{M\to\infty}\hat{H}_M, \tag{D1}$$

$$\hat{H}_M = \hat{H}_{imp} + \sqrt{\frac{\Gamma}{\pi}}(\hat{d}^{+}\hat{a}_0 + \hat{a}^{+}_0\hat{d}) + \sum_{n=0}^{M-1} t_n(\hat{a}^{+}_n\hat{a}_{n+1} + \hat{a}^{+}_{n+1}\hat{a}_n), \tag{D2}$$

where each site ($\hat{a}_n$) couples only to its nearest neighbors ($\hat{a}_{n-1}$, $\hat{a}_{n+1}$) and the couplings (t_{n-1}, t_n) decay exponentially along the chain. (The exact expression for t_n can be found in, for example, Refs. 25 and 27. Also, since we are in the wide band limit, on-site terms $\epsilon_n\hat{a}^{+}_n\hat{a}_n$ do not appear in Eq. (D2).) If we start with the 0th site and we continue through the Mth site on the chain, let the renormalized Hamiltonians be denoted $\hat{H}_0, \hat{H}_1, \ldots, \hat{H}_M$. For a finite temperature calculation, we stop at the Mth site, where the coupling t_{M-1} between sites $M-1$ and M is order of kT; at zero temperature, we stop at the Mth site, where the eigenvalues of $\hat{H}_M$ have reached a fixed point. We then use $\hat{H}_M$ as an approximation of the total Hamiltonian, $\hat{H} \approx \hat{H}_M$.[25,27]

The standard NRG approach for calculating observables of a single resonant model is very well known,[25,27] and is particularly straightforward in the wide band approximation. Between the single resonant model and the standard Anderson-Holstein model, the only difference is the impurity Hamiltonian ($\hat{H}_{imp}$): for the single resonant model, $\hat{H}_{imp} = E_d\hat{d}^{+}\hat{d}$, whereas for the standard AH model, $\hat{H}_{imp} = \hat{H}_s$ (Eq. (3)), which consists of both electron and phonon states (and the latter must be truncated, usually using a basis of Harmonic oscillators).[26,49]

Now, if we want to go beyond the standard Anderson-Holstein model and include a position-dependent hybridization $\Gamma(x)$ as in Eq. (A2), the standard NRG approach does require a small modification. Namely, when constructing the Hamiltonian that includes site 0 on the chain, $\hat{H}_0 = \hat{H}_{imp} + \sqrt{\frac{\Gamma}{\pi}}(\hat{d}^{+}\hat{a}_0 + \hat{a}^{+}_0\hat{d})$, one must construct the correct matrix elements for $\Gamma(x)$. Otherwise, the rest of the standard algorithm applies: the inter-site couplings between sites 0 and 1, or sites 1 and 2, etc., are unchanged (since these couplings represent a discretization of the metal bath in the wide band approximation and are unrelated to the phonon). We have used this algorithm above and in Ref. 39.

Let us now discuss how one constructs the potential of mean force and local electronic populations in the context of an NRG calculation,

$$V_{NRG}(x) \approx -\frac{1}{\beta}\ln\langle x|Tr_e e^{-\beta\hat{H}_M}|x\rangle, \tag{D3}$$

$$n_{NRG}(x) \approx \frac{\langle x|Tr_e(\hat{d}^{+}\hat{d})_M e^{-\beta\hat{H}_M}|x\rangle}{\langle x|Tr_e e^{-\beta\hat{H}_M}|x\rangle}. \tag{D4}$$

Because the eigenstates of the Hamiltonian become mixed phonon and electronic states as one moves along the chain, it can be tricky to trace over the electronic DoFs and generate $V_{NRG}(x)$ and $n_{NRG}(x)$. Such a trace can be performed, however, if one keeps track of the transformation matrices S_N ($N = 1 \ldots M$) that diagonalize each renormalized Hamiltonian $\hat{H}_N$ ($N = 1 \ldots M$).

In such a case, starting from the Mth site density matrix $\hat{\rho}_M = \frac{1}{Z}\exp(-\beta\hat{H}_M)$, we use the transformation matrix S_M to transform $\hat{\rho}_M$ back to the $(M-1)$th eigenbasis and then trace over the Mth site electronic DoFs.[25,50] We iterate the same procedure all the way back to the 0th site basis, which consists of only the impurity electron and the phonon. We further trace over the impurity electronic degree of freedom to generate a purely nuclear density matrix in the original basis of phonon states, $\hat{\rho}_{red} \equiv Tr_e\hat{\rho}_M$. Similarly, for the local electronic population, we back transform the operator $(\hat{d}^{+}\hat{d})_M\hat{\rho}_M$ until we arrive at the operator $\hat{\Sigma} \equiv Tr_e(\hat{d}^{+}\hat{d})_M\hat{\rho}_M$. Now, in the original basis of phonon states, we diagonalize the position operator, and get the eigenvalue and eigenstates of the position operator, $\hat{x}|x_i\rangle = x_i|x_i\rangle$. We further note that the average electronic population is

$$\begin{aligned} N_{NRG} &= \sum_i \langle x_i|Tr_e(\hat{d}^{+}\hat{d})_M\hat{\rho}_M|x_i\rangle \\ &= \sum_i \frac{\langle x_i|Tr_e(\hat{d}^{+}\hat{d})_M\hat{\rho}_M|x_i\rangle}{\langle x_i|Tr_e\hat{\rho}_M|x_i\rangle}\frac{\langle x_i|Tr_e\hat{\rho}_M|x_i\rangle}{x_{i+1}-x_i}(x_{i+1}-x_i) \\ &\equiv \sum_i \frac{\langle x_i|\hat{\Sigma}|x_i\rangle}{\langle x_i|\hat{\rho}_{red}|x_i\rangle}\frac{\langle x_i|\hat{\rho}_{red}|x_i\rangle}{x_{i+1}-x_i}(x_{i+1}-x_i) \\ &\to \int n_{NRG}(x)\exp(-\beta V_{NRG}(x))dx. \end{aligned} \tag{D5}$$

The arrow in the above equation indicates going from a discrete limit to a continuous limit. Finally, we arrive at expressions for the potential of mean force and local population

in the context of an NRG calculation,

$$V_{NRG}(x_i) = -\frac{1}{\beta}\ln\frac{\langle x_i|\hat{\rho}_{red}|x_i\rangle}{x_{i+1}-x_i}, \tag{D6}$$

$$n_{NRG}(x_i) = \frac{\langle x_i|\hat{\Sigma}|x_i\rangle}{\langle x_i|\hat{\rho}_{red}|x_i\rangle}, \tag{D7}$$

that can be compared directly to our results from the PMF approach (Eq. (A3) and Eq. (16)). Note that the spacing between the eigenvalues of the position operator $(x_{i+1} - x_i)$ will not usually be uniform, so that it is crucial to include the term $x_{i+1} - x_i$ in Eq. (D6).

APPENDIX E: *AD HOC* POST-DYNAMICAL BROADENING

If we are interested in dynamics (and not just statics), it is important to note that there is an alternative approach that is entirely different from the MF and PMF algorithms presented in the body of this paper. For large temperature ($kT \gg \Gamma$), we can ignore broadening to zeroth order, and one can use a simple classical master equation[39,41,46] to study coupled nuclear electronic dynamics,

$$\hbar\frac{\partial P_0(x,p,t)}{\partial t} = -\hbar\omega p\frac{\partial P_0(x,p,t)}{\partial x} + \hbar\omega x\frac{\partial P_0(x,p,t)}{\partial p} - \Gamma f P_0(x,p,t) + \Gamma(1-f)P_1(x,p,t), \tag{E1}$$

$$\hbar\frac{\partial P_1(x,p,t)}{\partial t} = -\hbar\omega p\frac{\partial P_1(x,p,t)}{\partial x} + (\hbar\omega x + \sqrt{2}g)\frac{\partial P_1(x,p,t)}{\partial p} + \Gamma f P_0(x,p,t) - \Gamma(1-f)P_1(x,p,t), \tag{E2}$$

where $P_0(x,p,t)$ ($P_1(x,p,t)$) describes the density probability with an electron occupied (unoccupied) in the molecule and an oscillator has a momentum p and position x. According to Eqs. (E1) and (E2), one runs classical trajectories on two different surfaces, with hops proportional to Γ and the Fermi function, $f = \frac{1}{\exp\beta\epsilon(x)+1}$.

At equilibrium, the solutions to the AH model can be calculated analytically and we can extract populations to compare against the relevant data in Figs. 3 and 4:

$$P_0^{eq}(x,p) = C\exp\left(-\frac{1}{2}\beta\hbar\omega(x^2+p^2)\right), \tag{E3}$$

$$P_1^{eq}(x,p) = C\exp\left(-\frac{1}{2}\beta\hbar\omega(x^2+p^2) - \beta\epsilon(x)\right). \tag{E4}$$

Here, C is a normalization factor given by $\int\int dxdp\left(P_0^{eq}(x,p) + P_1^{eq}(x,p)\right) = 1$. More explicitly, $C = \frac{\beta\hbar\omega}{2\pi}\frac{1}{1+\exp(-\beta(E_d - g^2/\hbar\omega))}$. The impurity electronic population becomes

$$N = \int dxdpP_1^{eq}(x,p) = f(\bar{E}_d), \tag{E5}$$

where $\bar{E}_d \equiv E_d - g^2/\hbar\omega$ is the renormalized impurity energy. Thus, according to Eq. (E5), the electronic population is a simple Fermi function with the renormalized impurity energy level $\bar{E}_d$; no broadening is included in Eq. (E5).

At this point, if we want to include broadening and study lower temperatures, we have previously[39,41] presented the following two alternatives:

1. The first approach, which we refer to as "broadening 1," simply broadens the electronic population by Γ,

$$N = \int\frac{dE}{2\pi}\frac{\Gamma}{(E-\bar{E}_d)^2 + (\Gamma/2)^2}f(E). \tag{E6}$$

2. The second approach, which we refer to as "broadening 2," broadens the electronic population by a total Marcus rate γ_t[39]

$$N = \int\frac{dE}{2\pi}\frac{\gamma_t}{(E-\bar{E}_d)^2 + (\gamma_t/2)^2}f(E). \tag{E7}$$

Here, γ_t is the sum of forward ($k_{1\to0}$) and backward ($k_{0\to1}$) electron transfer rates, $\gamma_t \equiv k_{0\to1} + k_{1\to0}$, with

$$k_{1\to0} = \int dx\Gamma(1 - f(\sqrt{2}gx + E_d)) \times\sqrt{\frac{\hbar\omega}{2\pi kT}}e^{-\frac{1}{2}\hbar\omega(x+\sqrt{2}g/\hbar\omega)^2/kT}, \tag{E8}$$

$$k_{0\to1} = \int dx\Gamma f(\sqrt{2}gx + E_d)\sqrt{\frac{\hbar\omega}{2\pi kT}}e^{-\frac{1}{2}\hbar\omega x^2/kT}. \tag{E9}$$

We note that the mean field approach (Eq. (9)) and broadening 1 (Eq. (E6)) are applicable only for a constant Γ, while broadening 2 (Eq. (E7)) can be extended to the case whereby Γ depends on nuclear position x.

In Figs. 4-9, we show that Eqs. (E6) and (E7) are reasonable but not as good at computing electronic population as compared with our PMF approach. However, they do usually outperform MFT.

APPENDIX F: A PROOF OF THE RELATIONSHIP BETWEEN THE MULTIPLE SOLUTIONS OF MFT AND EXISTENCE OF A PMF POTENTIAL BARRIER FOR THE SYMMETRIC CASE

Here, we prove the claim from Sec. VI B that, for the symmetric AH model, the critical value of g (above which one finds multiple solutions for the electronic population in a MFT) is exactly the same value of g that gives a finite (nonzero) energy barrier according to a potential of mean force. We note that, because the Hamiltonian is symmetric ($E_d = E_r$), we always have the simple solution for electronic population, $N = 0.5$. If $\frac{dN}{dE_d}|_{E_d=Er,N=0.5} > 0$, we will have multiple solutions. Thus, we take the derivative with respect to E_d on both sides of Eq. (9), and we find

$$\frac{dN}{dE_d} = \int\frac{dE}{2\pi}\frac{-2(E - E_d + 2E_rN)(-1 + 2E_r\frac{dN}{dE_d})\Gamma}{((E - E_d + 2E_rN)^2 + (\Gamma/2)^2)^2}f(E). \tag{F1}$$

If we rearrange the above equation, and use $E_d = E_r$, $N = 0.5$, we find

$$\left(1 + E_r\int\frac{dE}{2\pi}\frac{4E\Gamma}{(E^2 + (\Gamma/2)^2)^2}f(E)\right)\frac{dN}{dE_d} = \int\frac{dE}{2\pi}\frac{2E\Gamma}{(E^2 + (\Gamma/2)^2)^2}f(E). \tag{F2}$$

Since the right hand side of the above equation is less than zero, and $\frac{dN}{dE_d}|_{E_d=E_r,N=0.5} > 0$, we have

$$1 + E_r \int \frac{dE}{2\pi} \frac{4E\Gamma}{(E^2 + (\Gamma/2)^2)^2} f(E) < 0. \tag{F3}$$

Eq. (F3) is the precise condition that stipulates when we will find multiple solutions for the electronic population in a MFT. At zero temperature, Eq. (F3) reduces to $E_r > \pi\Gamma/4$.

We now consider the occurrence of a barrier for the potential of mean force (Eq. (17)); as before, we focus on the simplest symmetric case, $E_d = E_r$. The first derivative of the PMF over x is

$$\frac{\partial V(x)}{\partial x} = \hbar\omega x + \sqrt{2}g \times \int \frac{dE}{2\pi} \frac{\Gamma}{(E - \sqrt{2}gx - E_d)^2 + (\Gamma/2)^2} f(E). \tag{F4}$$

The PMF in Eq. (F4) reaches an extremum at $x = x_1/2 = -\sqrt{2}g/2\hbar\omega$, because $\frac{\partial V(x)}{\partial x}|_{E_d=E_r,x=x_1/2} = 0$. This extremum is a barrier if

$$\frac{\partial^2 V(x)}{\partial x^2}|_{x=x_1/2} = \hbar\omega + \sqrt{2}g \int \frac{dE}{2\pi} \frac{2E\sqrt{2}g\Gamma}{(E^2 + (\Gamma/2)^2)^2} f(E) < 0. \tag{F5}$$

Or, in other words,

$$1 + E_r \int \frac{dE}{2\pi} \frac{4E\Gamma}{(E^2 + (\Gamma/2)^2)^2} f(E) < 0. \tag{F6}$$

The agreement between Eqs. (F3) and (F6) proves the hypothesis above for the symmetric case.

[1]A. Nitzan and M. A. Ratner, Science **300**, 1384 (2003).
[2]C. Joachim, J. K. Gimzewski, and A. Aviram, Nature **408**, 541 (2000).
[3]R. H. M. Smit, Y. Noat, C. Untiedt, N. D. Lang, M. C. van Hemert, and J. M. van Ruitenbeek, Nature **419**, 906 (2002).
[4]T. Lee, W. Wang, J. F. Klemic, J. J. Zhang, J. Su, and M. A. Reed, J. Phys. Chem. B **108**, 8742 (2004).
[5]D. J. Wold and C. D. Frisbie, J. Am. Chem. Soc. **123**, 5549 (2001).
[6]S. Datta, W. Tian, S. Hong, R. Reifenberger, J. I. Henderson, and C. P. Kubiak, Phys. Rev. Lett. **79**, 2530 (1997).
[7]K. Slowinski, R. V. Chamberlain, C. J. Miller, and M. Majda, J. Am. Chem. Soc. **119**, 11910 (1997).
[8]D. Segal and A. Nitzan, J. Chem. Phys. **122**, 194704 (2005).
[9]J. Chen, M. A. Reed, A. M. Rawlett, and J. M. Tour, Science **286**, 1550 (1999).
[10]I. Amlani, A. M. Rawlett, L. A. Nagahara, and R. K. Tsui, Appl. Phys. Lett. **80**, 2761 (2002).
[11]K. Walzer, E. Marx, N. C. Greenham, R. J. Less, P. R. Raithby, and K. Stokbro, J. Am. Chem. Soc. **126**, 1229 (2004).
[12]C. Li, D. Zhang, X. Liu, S. Han, T. Tang, C. Zhou, W. Fan, J. Koehne, J. Han, M. Meyyappan, A. M. Rawlett, D. W. Price, and J. M. Tour, Appl. Phys. Lett. **82**, 645 (2003).
[13]T. L. Schull, J. G. Kushmerick, C. H. Patterson, C. George, M. H. Moore, S. K. Pollack, and R. Shashidhar, J. Am. Chem. Soc. **125**, 3202 (2003).
[14]J. Chen, J. Su, W. Wang, and M. Reed, Phys. E **16**, 17 (2003).
[15]M. Galperin, M. A. Ratner, and A. Nitzan, Nano Lett. **5**, 125 (2005).
[16]L. Simine and D. Segal, J. Chem. Phys. **141**, 014704 (2014).
[17]M. Galperin, M. A. Ratner, and A. Nitzan, J. Phys.: Condens. Matter **19**, 103201 (2007).
[18]B. K. Agarwalla, J.-H. Jiang, and D. Segal, Phys. Rev. B **92**, 245418 (2015).
[19]T. Holstein, Ann. Phys. **8**, 325 (1959).
[20]M. Thoss, I. Kondov, and H. Wang, Phys. Rev. B **76**, 153313 (2007).
[21]K. F. Albrecht, H. Wang, L. Mühlbacher, M. Thoss, and A. Komnik, Phys. Rev. B **86**, 081412 (2012).
[22]E. Y. Wilner, H. Wang, G. Cohen, M. Thoss, and E. Rabani, Phys. Rev. B **88**, 045137 (2013).
[23]E. Y. Wilner, H. Wang, M. Thoss, and E. Rabani, Phys. Rev. B **89**, 205129 (2014).
[24]E. Lörtscher, J. W. Ciszek, J. Tour, and H. Riel, Small **2**, 973 (2006).
[25]R. Bulla, T. A. Costi, and T. Pruschke, Rev. Mod. Phys. **80**, 395 (2008).
[26]A. C. Hewson and D. Meyer, J. Phys.: Condens. Matter **14**, 427 (2002).
[27]K. G. Wilson, Rev. Mod. Phys. **47**, 773 (1975).
[28]N. Bode, S. V. Kusminskiy, R. Egger, and F. von Oppen, Beilstein J. Nanotechnol. **3**, 144 (2012).
[29]M. Thomas, T. Karzig, S. V. Kusminskiy, G. Zaránd, and F. von Oppen, Phys. Rev. B **86**, 195419 (2012).
[30]D. Mozyrsky, M. B. Hastings, and I. Martin, Phys. Rev. B **73**, 035104 (2006).
[31]M. Brandbyge, P. Hedegård, T. F. Heinz, J. A. Misewich, and D. M. Newns, Phys. Rev. B **52**, 6042 (1995).
[32]F. Pistolesi, Y. M. Blanter, and I. Martin, Phys. Rev. B **78**, 085127 (2008).
[33]R. Englman and J. Jortner, Mol. Phys. **18**, 145 (1970).
[34]N. R. Kestner, J. Logan, and J. Jortner, J. Phys. Chem. **78**, 2148 (1974).
[35]R. A. Marcus, Ann. Rev. Phys. Chem. **15**, 155 (1964).
[36]R. A. Marcus, J. Chem. Phys. **24**, 966 (1956).
[37]R. A. Marcus, J. Chem. Phys. **43**, 679 (1965).
[38]A. Nitzan, Ann. Rev. Phys. Chem. **52**, 681 (2001).
[39]W. Dou, A. Nitzan, and J. E. Subotnik, J. Chem. Phys. **142**, 234106 (2015).
[40]G. D. Mahan, *Many-Particle Physics* (Plenum, New York, 2000).
[41]W. Dou, A. Nitzan, and J. E. Subotnik, J. Chem. Phys. **142**, 084110 (2015).
[42]W. Dou, A. Nitzan, and J. E. Subotnik, J. Chem. Phys. **143**, 054103 (2015).
[43]J. E. Subotnik, T. Hansen, M. A. Ratner, and A. Nitzan, J. Chem. Phys. **130**, 144105 (2009).
[44]For NRG calculations here and below, the basis is initialized with 160 boson states, the maximum number of eigenstates kept is $N_s = 2000$, and the logarithmic discretizing parameter is $\Lambda = 2$.
[45]M. Galperin and A. Nitzan, J. Phys. Chem. Lett. **6**, 4898 (2015).
[46]F. Elste, G. Weick, C. Timm, and F. von Oppen, Appl. Phys. A **93**, 345 (2008).
[47]W. Dou and J. E. Subotnik, J. Chem. Phys. **144**, 024116 (2016).
[48]H. Haug and A. Jauho, *Quantum Kinetics in Transport and Optics of Semiconductors* (Springer, New York, 2007).
[49]A. Jovchev and F. B. Anders, Phys. Rev. B **87**, 195112 (2013).
[50]F. B. Anders and A. Schiller, Phys. Rev. Lett. **95**, 196801 (2005).